Journal of Chromatography, 454 (1988) 1–21
Elsevier Science Publishers B.V., Amsterdam — Printed in The Netherlands

CHROM. 20 816

THEORETICAL OPTIMIZATION OF OPERATING PARAMETERS IN NON-IDEAL DISPLACEMENT CHROMATOGRAPHY

MICHAEL W. PHILLIPS, GUHAN SUBRAMANIAN and STEVEN M. CRAMER*
Bioseparations Research Center, Department of Chemical Engineering, Rensselaer Polytechnic Institute, Troy, NY 12180-3590 (U.S.A.)
(First received April 18th, 1988; revised manuscript received July 19th, 1988)

SUMMARY

A mathematical model was developed for the simulation of non-ideal displacement chromatography. The model incorporates finite mass transport to the solid adsorbent by using a linear driving force approximation with a coupled external film and internal pore mass transfer coefficient. Equilibrium adsorption at the fluid–solid interface is described using competitive langmuirian adsorption isotherms. A finite difference numerical technique was employed to approximate the system of coupled, non-linear partial differential equations. The model was used to simulate the effluent concentration profiles under various displacement chromatographic conditions. The effects of axial dispersion and finite mass transport were examined by varying the Peclet and Stanton numbers, respectively. Slow mass transfer rates were shown to have a dispersive effect on the shock waves generated in displacement chromatography, resulting in greater zone overlap. Constant pattern formation was observed under non-ideal conditions. The throughput obtained in displacement chromatography was examined as a function of feed load, flow velocity, and displacer concentration. For non-ideal systems, the throughput was shown to exhibit a maximum at unique values of these operating parameters. The effects of particle diameter and solute diffusivity on the throughput were also examined. Model predictions indicate that the use of large particles could be detrimental to the performance of displacement systems when high velocities are employed. For macromolecular separations by displacement chromatography, small particles are required regardless of the linear velocity. The model presented here is a useful tool for the optimization and scale-up of displacement chromatographic processes.

INTRODUCTION

Displacement chromatography is rapidly evolving into a powerful preparative bioseparation technique due to the high throughput and product purity associated with the process. The separation is based on competition of the components for adsorption sites on the stationary phase and the process takes advantage of the non-linearity of the isotherms. Although the physicochemical basis of displacement chromatography was established by Tiselius in 1943[1], the full potential of this

0021-9673/88/$03.50 © 1988 Elsevier Science Publishers B.V.

technique was not fully realized until the recent work by Horváth and co-workers[2–8].

In displacement chromatography, a front of displacer solution traveling behind the feed drives the separation of the feed components into adjacent pure zones which move at the same velocity as the displacer front. The concentration of each zone is determined solely by its adsorption isotherm and the concentration and isotherm of the displacer. The displacer must have a higher affinity for the stationary phase than any of the feed components[7].

In this method, the column is first equilibrated with an inert carrier solvent. The feed mixture is then introduced into the column followed by a step-change at the column inlet to a solution containing the displacer compound. Upon completion of the displacement process, the displacer is removed from the column by the passing of a suitable regenerant solution.

Displacement chromatography offers significant advantages in preparative chromatography as compared to the conventional elution mode[7]. Since displacement chromatography takes advantage of the non-linearity of the isotherms, a larger feed can be separated on a given column with the purified components recovered at significantly higher concentrations. Furthermore, the tailing observed in preparative-scale elution chromatography is greatly reduced in displacement chromatography due to the sharp zones formed in the process. These advantages are particularly significant for the isolation of biomolecules from relatively dilute solutions such as those encountered in biotechnology processes.

While the effects of axial dispersion and mass transport have been included in models of multicomponent adsorption[9–15], work on modeling displacement chromatography has been mainly limited to ideal chromatographic systems. Helfferich and Klein[16] and Helfferich[17,18] developed a model for displacement systems assuming equilibrium adsorption, plug flow, and constant separation factors. In their treatment, a so-called "*h*-transformation" was employed to convert the system of coupled partial differential equations to a set of algebraic equations. Rhee and co-workers[19,20] used a similar approach to solve the mass balance equations. Yu and Wang[21], and Geldart *et al.*[22], have used the "*h*-transform" technique to study the dynamics of elution and displacement ion-exchange chromatography. Frenz and Horváth[5] compared experimental displacement data obtained with analytical HPLC columns to the predictions of the ideal displacement model. Guiochon and Katti[23] have compared displacement and elution profiles obtained by numerically solving the mass balance equations. Morbidelli *et al.*[24,25] have used the pore diffusion model in their studies of gas adsorption separation processes.

To date, the theory of displacement in liquid chromatography (LC) applied only to conditions of ideal chromatography, neglecting the effects of dispersion and finite mass transport. However, the scale-up of the process with respect to stationary phase particle size, column dimensions, feed load, volumetric flow-rates, and molecular dimensions of the feed and displacer components may affect the effluent displacement profiles.

We have recently shown that the preparative separation of peptides, antibiotics, and proteins can be accomplished using high-performance liquid chromatography (HPLC) columns in the displacement mode[26]. We are presently investigating the scale-up of these displacement processes to larger column systems. In order to facilitate the scale-up of the process, it is important that a model be developed to predict the

effects of scale-up on the effluent displacement profiles. In this work, we present theoretical results on the simulation of displacement chromatography under chromatographic conditions which include the effects of axial dispersion and finite mass transfer.

THEORETICAL DEVELOPMENT

Consider an isothermal chromatographic column of constant void fraction, ε, through which an inert carrier containing N adsorbable species flows with a constant interstitial velocity, u_0. The system is assumed to be one dimensional in the direction of flow with uniform cross-sectional area. Let c_i denote the molar concentration of species i in the fluid phase and $\bar{q}_i$ represent the average concentration of species i in the stationary phase material. Let D_i and k_i represent the axial dispersion coefficient and the overall mass transfer coefficient of species i, respectively. The material balance for species i in the fluid phase can then be written as

$$\frac{\partial c_i}{\partial t} + u_0 \frac{\partial c_i}{\partial z} + \frac{1 - \varepsilon}{\varepsilon} \frac{\partial \bar{q}_i}{\partial t} - D_i \frac{\partial^2 c_i}{\partial z^2} = 0 \qquad i = 1, 2, \ldots, N \tag{1}$$

$$\frac{\partial \bar{q}_i}{\partial t} = k_i (q_i^* - \bar{q}_i) \qquad i = 1, 2, \ldots, N \tag{2}$$

where q_i^* represents the stationary phase concentration in the absence of mass transport limitations. The axial dispersion coefficient for species i, D_i, includes longitudinal spreading due to both molecular diffusion and eddy dispersion[27,28]. The stationary phase accumulation term, $\partial \bar{q}_i / \partial t$, is approximated using a linear driving force model which employs an overall effective mass transfer coefficient, k_i, to describe both the film and intraparticular mass transport.

It has been established that the equilibrium adsorption of most substances in chromatographic systems can be described by the langmuir adsorption isotherm[29–31]. For a multicomponent system, the langmuir isotherm for component i is given by

$$q_i^* = \frac{a_i c_i}{1 + \sum_{j=1}^{N} b_j c_j} \tag{3}$$

where a_i and b_i are the langmuir parameters for species i and N is the number of components in the mixture[30–32]. The system of equations described by eqns. 1 and 2 are coupled through this multicomponent adsorption isotherm.

Similar systems of equations have been solved numerically for multicomponent adsorption[9,14,15,31,33]. In order to use these equations to describe non-ideal displacement chromatography, the appropriate initial and boundary conditions must be employed. Specifically, the introduction of the feed, displacer, regenerant and carrier solutions must be represented by appropriate inlet boundary conditions.

Initially, the column is equilibrated with the inert carrier fluid. This initial state of the column can be represented as

$$c_i = \bar{q}_i = 0 \qquad \text{at } t = 0,\ 0 \leqslant z \leqslant L \tag{4}$$

$$i = 1, 2, \ldots, N$$

At $t = 0$, a feed solution containing $N - 1$ components at concentrations of c_{1F}, c_{2F}, ..., $c_{(N-1)F}$ is introduced into the column for a time t_{feed}. The inlet boundary conditions during the introduction of the feed are

$$u_0 c_i = u_0 c_{iF} + D_i \left.\frac{\partial c_i}{\partial z}\right|_{z=0} \qquad \text{at } z = 0,\ 0 \leqslant t \leqslant t_{feed} \tag{5}$$

$$i = 1, 2, \ldots, N - 1$$

and

$$c_N = 0 \qquad \text{at } z = 0,\ 0 \leqslant t \leqslant t_{feed} \tag{6}$$

Following the introduction of the feed, a solution containing only the displacer at a concentration c_{NF} is pumped into the column. The introduction of the displacer continues until time t_{displ}, the breakthrough time of the displacer at the column outlet. The inlet boundary conditions during the introduction of the displacer are

$$u_0 c_i = D_i \left.\frac{\partial c_i}{\partial z}\right|_{z=0} \qquad \text{at } z = 0,\ t_{feed} < t \leqslant t_{displ} \tag{7}$$

$$i = 1, 2, \ldots, N - 1$$

and

$$u_0 c_N = u_0 c_{NF} + D_N \left.\frac{\partial c_N}{\partial z}\right|_{z=0} \qquad \text{at } z = 0,\ t_{feed} < t \leqslant t_{displ} \tag{8}$$

The outlet boundary condition during the entire cycle of operation is given by

$$\left.\frac{\partial c_i}{\partial z}\right|_{z=L} = 0 \qquad \text{at } z = L,\ t \geqslant 0 \tag{9}$$

$$i = 1, 2, \ldots, N$$

A suitable regenerant scheme was also included in the model to calculate the time required to both remove the displacer from the column and to re-equilibrate the column with the inert carrier.

It is convenient to define the following dimensionless variables and parameters in order to facilitate the study of dispersion and mass transport effects in displacement systems:

$$\tau = \frac{u_0 t}{L},\ x = \frac{z}{L},\ Pe_i = \frac{u_0 L}{D_i},\ St_i = \frac{k_i L}{u_0}$$

where τ, x, Pe, and St represent dimensionless time, dimensionless axial position, Peclet number, and Stanton number, respectively. (Note: the fluid and stationary phase concentrations were kept in dimensional form in this model.)

Eqns. 1, 2, and 4–9 become, respectively,

$$\frac{\partial c_i}{\partial \tau} + \frac{\partial c_i}{\partial x} + \frac{1-\varepsilon}{\varepsilon}\frac{\partial \bar{q}_i}{\partial \tau} - \frac{1}{Pe_i}\frac{\partial^2 c_i}{\partial x^2} = 0 \qquad i = 1, 2, \ldots, N \tag{10}$$

$$\frac{\partial \bar{q}_i}{\partial \tau} = St_i\,(q_i^* - \bar{q}_i) \qquad i = 1, 2, \ldots, N \tag{11}$$

$$c_i = \bar{q}_i = 0 \qquad \text{at } \tau = 0,\ 0 \leqslant x \leqslant 1 \qquad i = 1, 2, \ldots, N \tag{12}$$

$$c_i = c_{iF} + \frac{1}{Pe_i}\left.\frac{\partial c_i}{\partial x}\right|_{x=0} \qquad \text{at } x = 0,\ 0 \leqslant \tau \leqslant \tau_{\text{feed}} \qquad i = 1, 2, \ldots, N-1 \tag{13}$$

$$c_N = 0 \qquad \text{at } x = 0,\ 0 \leqslant \tau \leqslant \tau_{\text{feed}} \tag{14}$$

$$c_i = \frac{1}{Pe_i}\left.\frac{\partial c_i}{\partial x}\right|_{x=0} \qquad \text{at } x = 0,\ \tau_{\text{feed}} < \tau \leqslant \tau_{\text{displ}} \qquad i = 1, 2, \ldots, N-1 \tag{15}$$

$$c_N = c_{NF} + \frac{1}{Pe_N}\left.\frac{\partial c_N}{\partial x}\right|_{x=0} \qquad \text{at } x = 0,\ \tau_{\text{feed}} < \tau \leqslant \tau_{\text{displ}} \tag{16}$$

$$\left.\frac{\partial c_i}{\partial x}\right|_{x=1} = 0 \qquad \text{at } x = 1,\ \tau \geqslant 0 \qquad i = 1, 2, \ldots, N \tag{17}$$

NUMERICAL PROCEDURE

A finite difference technique was employed to approximate the system of coupled, non-linear partial differential equations. The first order spatial and temporal derivatives were approximated using forward and backward differencing, respectively, and the second order spatial derivative was approximated using central differencing. Denoting the position of the node within the computational grid along the x and τ coordinates as m and n, respectively, eqns. 10 and 11 were combined and written as the following difference equations

$$c_i(m+1, n+1) = c_i(m, n+1) - \frac{\Delta x}{\Delta \tau}[c_i(m, n+1) - c_i(m, n)] +$$

$$- \frac{1-\varepsilon}{\varepsilon} \Delta x \, St_i [q_i^*(m, n+1) - \bar{q}_i(m, n)] +$$

$$+ \frac{1}{Pe_i \Delta x}[c_i(m+2, n) - 2c_i(m+1, n) + c_i(m, n)] \quad (18)$$

$$\bar{q}_i(m, n+1) = \Delta \tau \, St_i [q_i^*(m, n+1) - \bar{q}_i(m, n)] + \bar{q}_i(m, n) \quad (19)$$

The stability of the finite difference numerical scheme was evaluated for ideal displacement chromatography. Under these conditions, the steepest concentration gradients are produced, thus making this a useful test of stability in these systems. From a von Neumann analysis[34] the stability criterion was found to be

$$\psi = \frac{\Delta x}{u_{\min} \Delta \tau} \leqslant 1 \quad (20)$$

where $u_{\min}$ is the ratio of the minimum velocity of any species moving within the column to the interstitial velocity, u_0. In this study, the value of ψ was always less than 0.8 to assure stable solutions.

A FORTRAN program was written to march through the resulting difference equations. The program was initiated with the following parameters: spatial (Δx) and temporal ($\Delta \tau$) step increments, τ_{feed}, u_0, column dimensions, ε, isotherm parameters and input concentrations of all species, and the characteristic Peclet and Stanton numbers. The isotherm parameters of the feed components and the displacer compound employed in this study are given in Table I. These parameters are representative of those obtained in experimental studies of the displacement chromatography of small biomolecules[5]. The operating parameters employed in the various simulation experiments are given in Table II. In all cases, the Peclet and Stanton numbers specified in this table represent the values for each component. The effect of increasing mass transport resistance was studied by varying the Stanton number in displacement simulations 1–3. The effect of axial dispersion was examined in simulations 4 and 5. In simulations 6–10, the column length was varied from 10 to 50 cm to examine the displacement development patterns produced in systems with axial dispersion and finite mass transport.

TABLE I

LANGMUIR PARAMETERS

Component	*a*	*b* (mM^{-1})
1	3.297	0.0905
2	4.200	0.1100
3	5.740	0.1247
4	9.203	0.1501

TABLE II

SIMULATION PARAMETERS

Unless otherwise stated, all displacement simulations used: u_0 = 1 cm/min, ε = 0.6, L = 25 cm, column inner diameter = 4.6 mm, Δx = 0.0004, $\Delta\tau$ = 0.00125; feed mixture, 10 mM each of components 1 and 3; displacer, component 4 at a concentration of 40 mM.

Displacement simulation run	τ_{feed}	*St*	*Pe*
1*	0.24	1600	1000 000
2*	0.24	800	1000 000
3*	0.24	200	1000 000
4*	0.24	1600	1000 000
5*	0.24	1600	30 000
6**,***	0.09	800	30 000
7**,***	0.09	800	30 000
8**,***	0.09	800	30 000
9**,***	0.09	800	30 000
10**,***	0.09	800	30 000
11	0.12–1.20	800	1000 000
12	0.12–1.20	300	30 000
13§	0.24	800	1000 000
14§	0.24	300	30 000
15	0.24	50–800	13 750–36 970
16	0.24	40–1600	100 000
17	0.24	5–1600	100 000

* Δx = 0.0002 and $\Delta\tau$ = 0.000625.

** Feed mixture contained 10 mM each of components 1, 2, and 3.

*** Column lengths of 10, 20, 30, 40, and 50 cm, were employed in displacement simulations 1, 2, 3, 4, and 5, respectively.

§ Displacer concentrations of 15, 30, 40, 60, 80, 100, and 140 mM were used to generate the throughput curves.

The model was used to both generate displacement effluent profiles under various conditions and to calculate the throughput obtained in these displacement systems. The throughput is defined as the mass of product isolated per unit time at a specified level of purity. The throughput for each species was calculated by numerically summing all fractions containing the component at a purity greater than 98% and dividing this by the total displacement cycle time which includes the introduction of feed, displacer, regenerant and carrier solutions.

Throughput curves were generated in simulations 11–17. The effect of increasing feed volumes at various levels of non-ideality was studied in runs 11 and 12. In simulations 13 and 14, the effect of increasing displacer concentration on product throughput was examined at various levels of chromatographic non-ideality. Simulation 15 examined the effect of increasing interstitial velocity on the throughput under both ideal and non-ideal displacement conditions. The throughput curve for the non-ideal system in simulation 15 was generated by assuming a constant mass transfer coefficient of k = 0.53 s^{-1} and an axial dispersion coefficient which varied with velocity according to the treatment of Horváth and Lin[27,28]

$$D = D_m + \frac{\lambda d_p u_0}{1 + \omega \left(\frac{d_p u_0}{D_m}\right)^{-1/3}} \tag{21}$$

where D_m is the solute molecular diffusivity, d_p is the stationary phase particle diameter, λ is a measure of the flow inequality in the bed, and ω is a function of the bed porosity. The subscript i has been omitted to simplify the expression. Values of $2 \cdot 10^{-5}$ cm^2/s, $5 \cdot 10^{-4}$ cm, 2.5, and 2.0 were used for D_m, d_p, λ, and ω, respectively.

The influence of mass transfer limitations on product throughput were investigated as a function of particle diameter, interstitial velocity, and solute diffusivity in simulation runs 16 and 17. The expression for the overall mass transfer coefficient used in this study was[31]

$$\frac{1}{kK} = \frac{d_p}{6k_f} + \frac{d_p^2}{60\ \varepsilon_p D_p} \tag{22}$$

where K is the equilibrium partition coefficient, k_f is the film mass transfer coefficient, ε_p is the intraparticular porosity, and D_p is the intraparticular diffusion coefficient.

The film mass transfer coefficient and the intraparticular diffusivity can be written using the expressions of Horváth and Lin[27,28]

$$k_f = \frac{\Omega D_m}{d_p}\left(\frac{d_p u_0}{D_m}\right)^{1/3} \tag{23}$$

$$D_p = \frac{D_m\ \varepsilon_p}{\theta} \tag{24}$$

where θ is the tortuosity factor and Ω is a function of the interparticular bed porosity.

Eqns. 22 through 24 were combined to obtain an expression for the Stanton number:

$$St = \frac{D_m L}{u_0 K d_p^2}\left[\frac{1}{\frac{1}{6\Omega}\left(\frac{D_m}{d_p u_0}\right)^{1/3} + \frac{\theta}{60\ \varepsilon_p^2}}\right] \tag{25}$$

In this study, values of 5.0, 0.5, 2.0, and 7.5 were used for K, ε_p, θ, and Ω, respectively.

RESULTS AND DISCUSSIONS

The effects of axial dispersion and finite mass transport in multicomponent adsorption systems have been studied by several authors[9-15]. In this work, we examine the effect of these non-idealities on the effluent concentration profiles obtained in simulations of displacement chromatography.

The effect of mass transfer limitations on the displacement effluent profile was investigated by varying the Stanton number. For a Stanton number of 1600, the

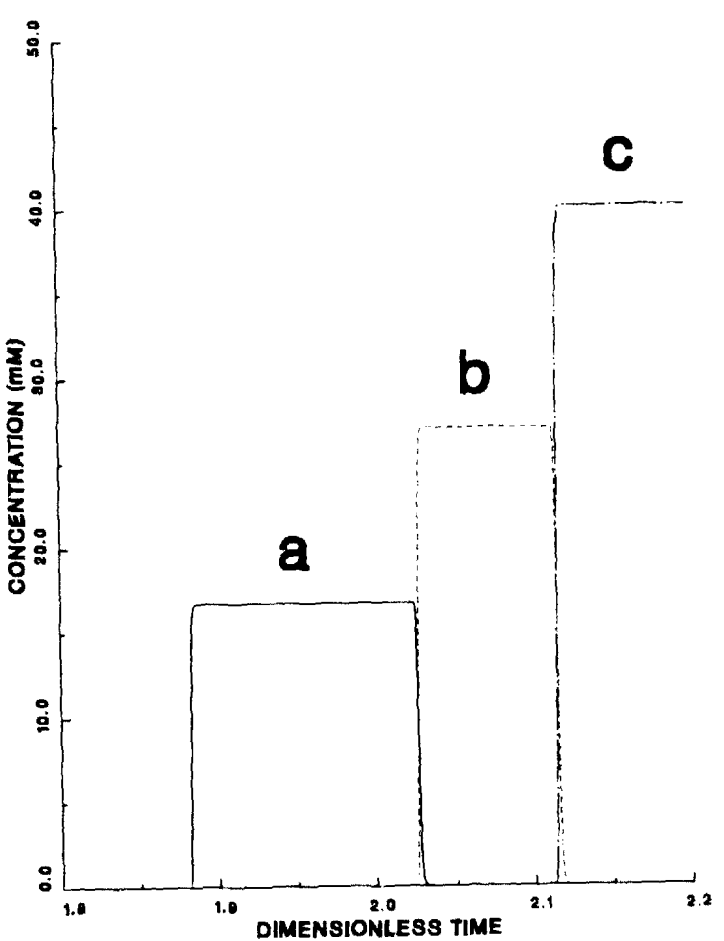

Fig. 1. Effluent displacement profile obtained with a Stanton number of 1600. Simulation conditions are described in Table II for run 1. a = Component 1; b = component 3; c = component 4 (displacer).

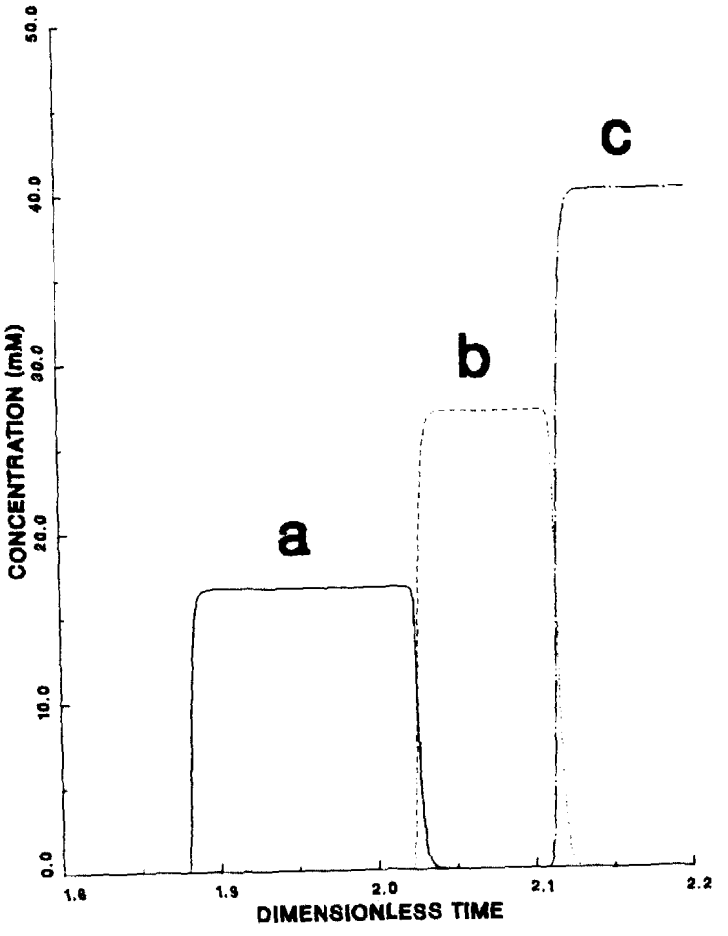

Fig. 2. Effluent displacement profile obtained with Stanton number of 800. Simulation conditions are described in Table II for run 2. Symbols as described in Fig. 1.

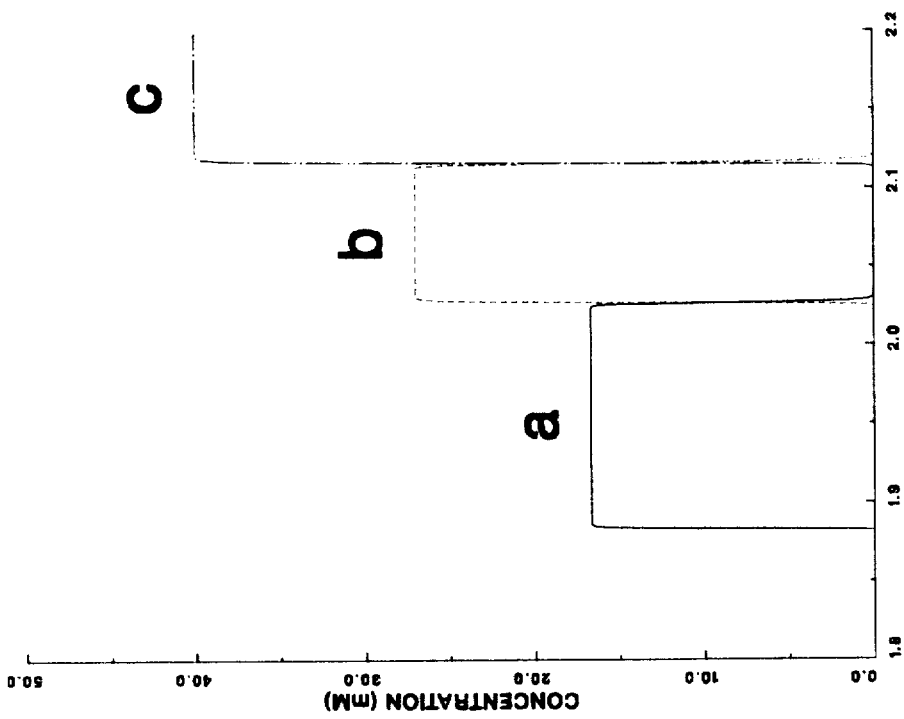

Fig. 3. Effluent displacement profile obtained with a Stanton number of 200. Simulation conditions are described in Table II for run 3. Symbols as described in Fig. 1.

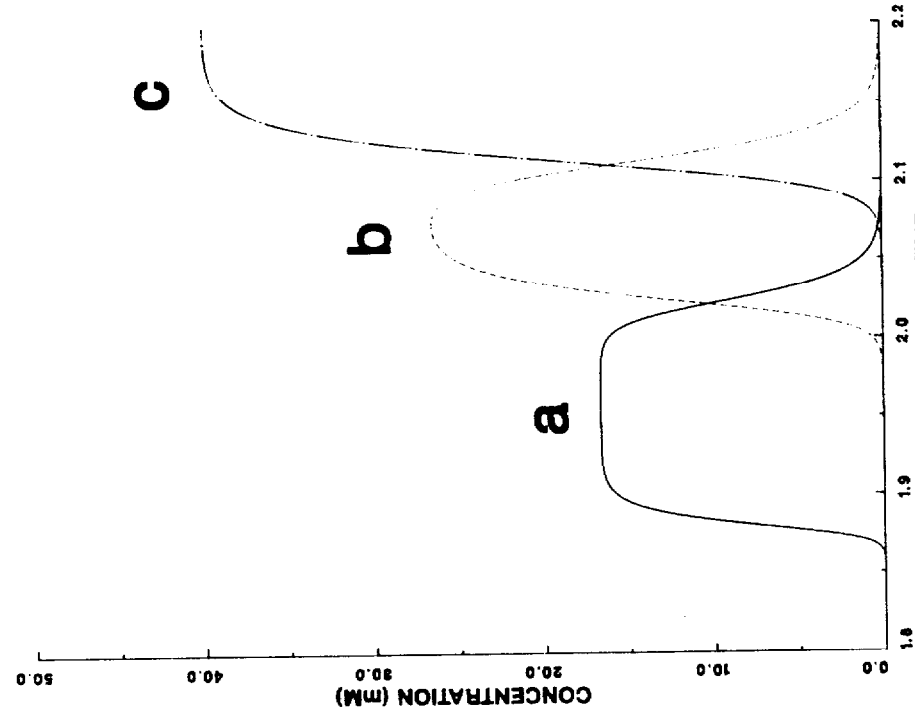

Fig. 4. Effluent displacement profile obtained with a Peclet number of 1000 000. Simulation conditions are described in Table II for run 4. Symbols as described in Fig.

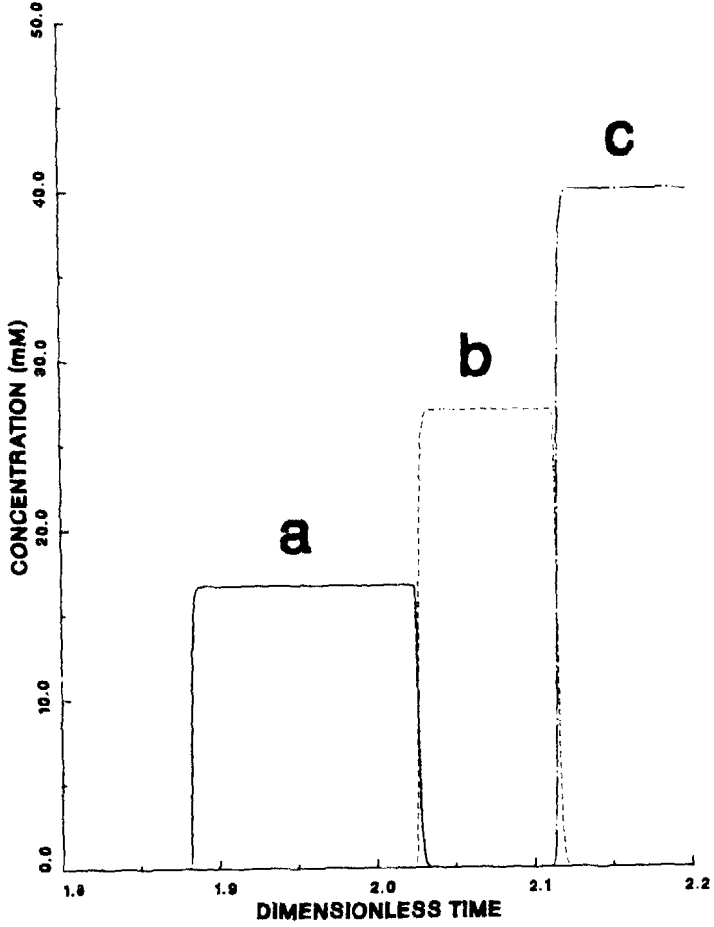

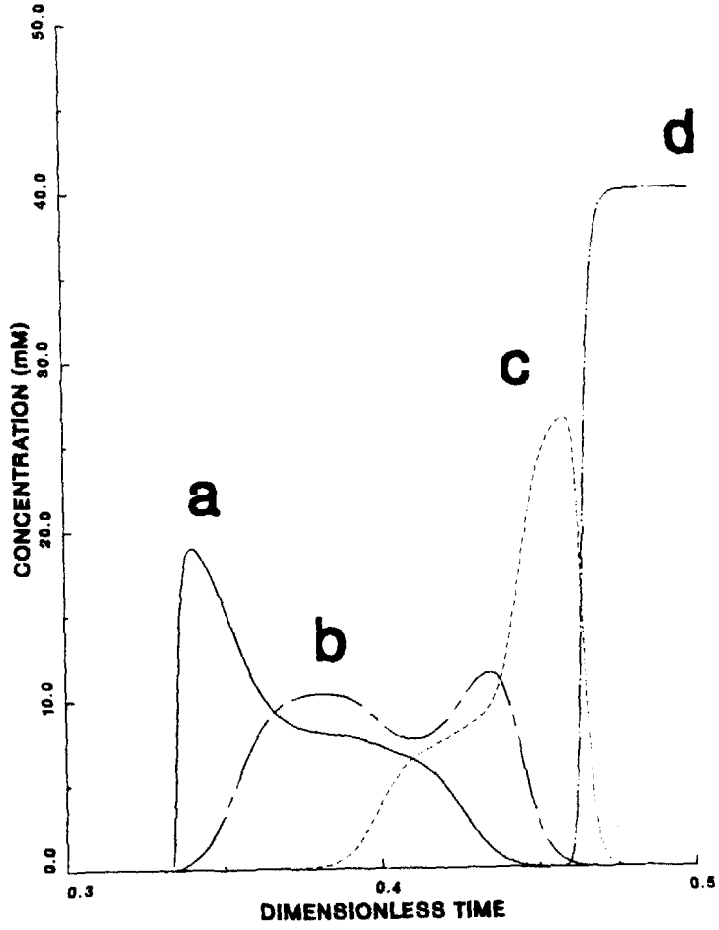

Fig. 5. Effluent displacement profile obtained with a Peclet number of 30 000. Simulation conditions are described in Table II for run 5. Symbols as described in Fig. 1.

Fig. 6. Effluent displacement profile obtained with a column length of 10 cm. Simulation conditions are described in Table II for run 6. a = Component 1; b = component 2; c = component 3; d = component 4 (displacer).

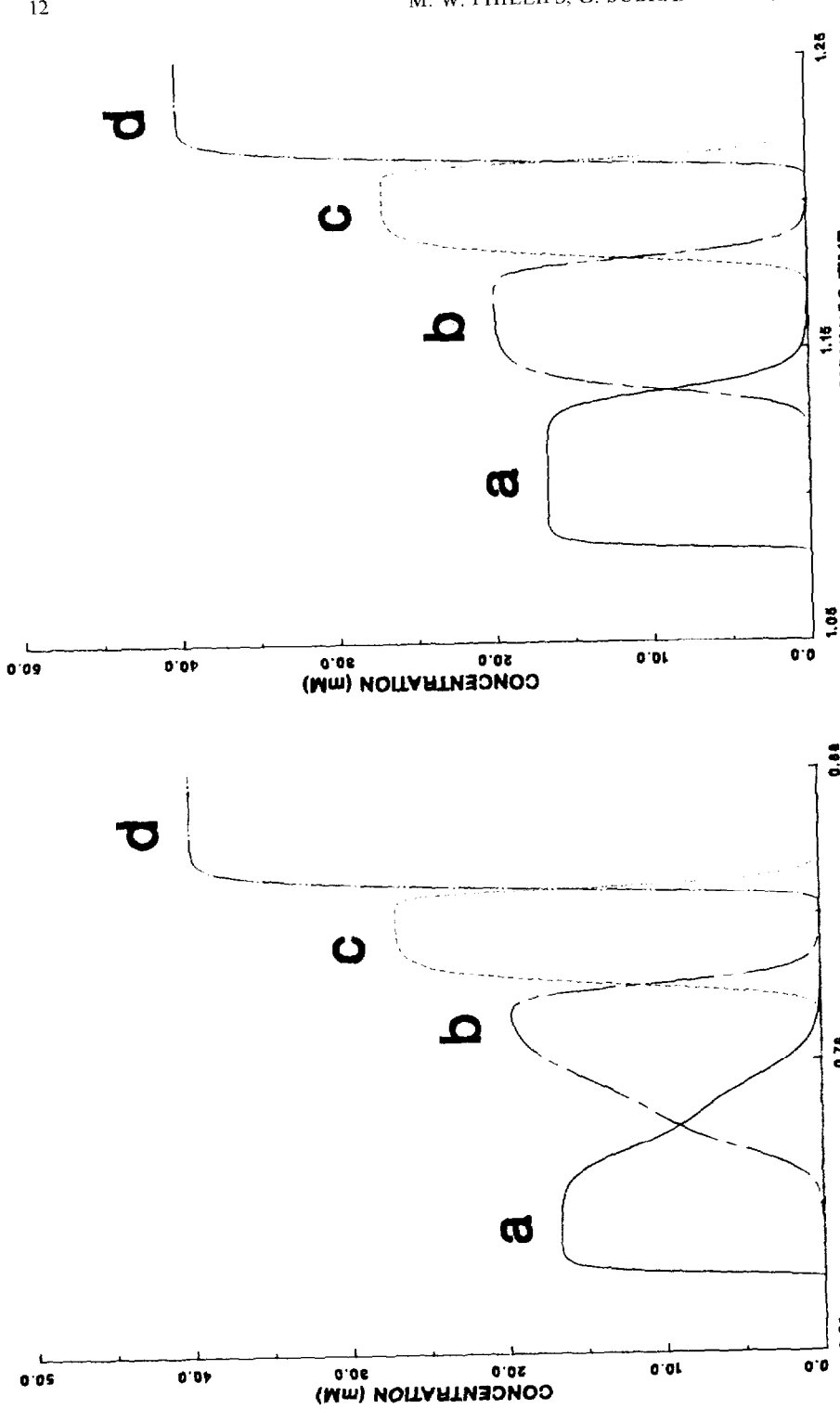

Fig. 7. Effluent displacement profile obtained with a column length of 20 cm. Simulation conditions are described in Table II for run 7. Symbols as described in Fig. 6.

Fig. 8. Effluent displacement profile obtained with a column length of 30 cm. Simulation conditions are described in Table II for run 8. Symbols as described in Fig. 6.

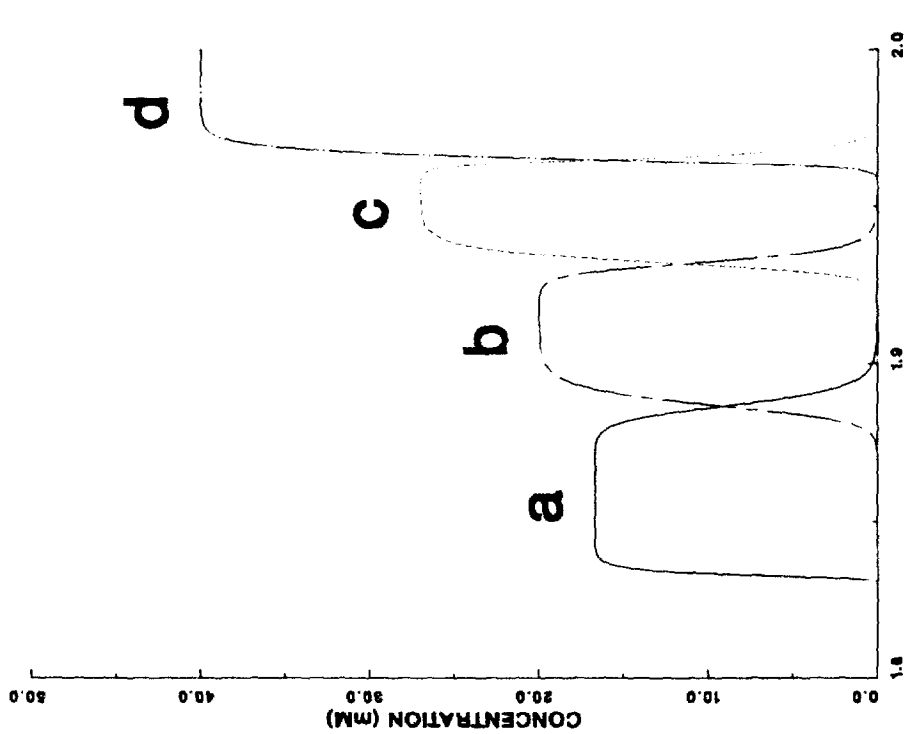

Fig. 9. Effluent displacement profile obtained with a column length of 40 cm. Simulation conditions are described in Table II for run 9. Symbols as described in Fig. 6.

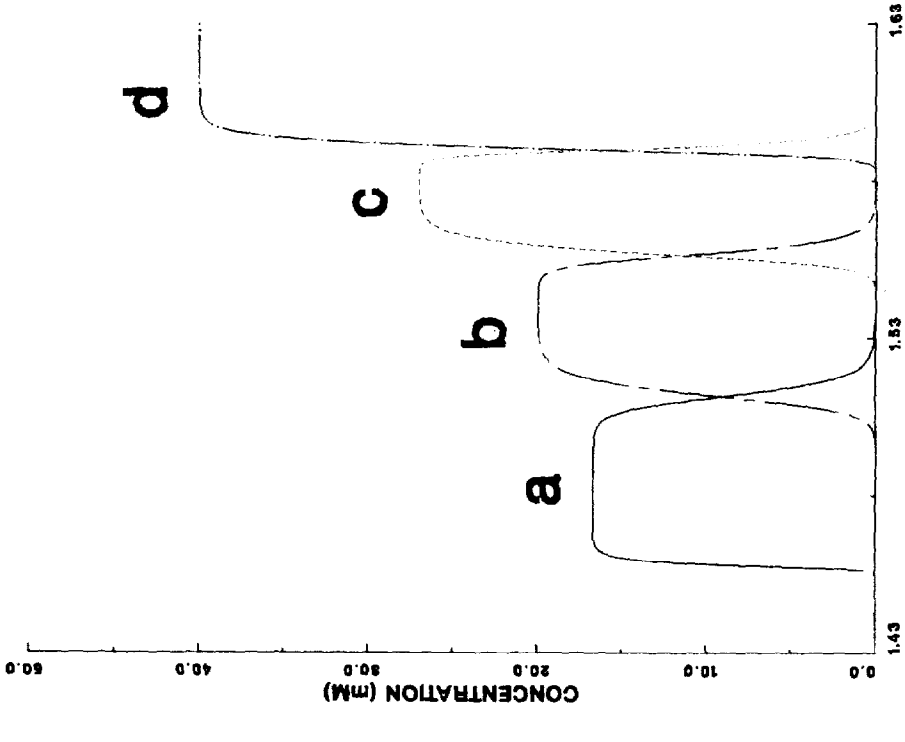

Fig. 10. Effluent displacement profile obtained with a column length of 50 cm. Simulation conditions are described in Table II for run 10. Symbols as described in Fig. 6.

displacement effluent profile approached that obtained under ideal chromatographic conditions as shown in Fig. 1. When the Stanton number is decreased to 800, the concentration shock waves separating the displacement zones become more diffuse, resulting in increased zone overlap as illustrated in Fig. 2. This result is dramatically depicted in Fig. 3, which shows the effluent profile for a Stanton number of 200. Under these conditions, the mass transport limitations result in excessive zone overlap, significantly decreasing the amount of purified material obtained in the separation process. Clearly, mass transport effects can play a major role in displacement chromatography.

The column Peclet number was varied to study the effect of axial dispersion in displacement chromatography. For Peclet numbers normally encountered in analytical liquid chromatography (30 000–1000 000), the axial dispersion was found to have little effect on the profiles as illustrated in Figs. 4 and 5. For large particles, a Peclet number on the order of 5000 is obtained. Under these conditions, the model also shows little effect of axial dispersion on the displacement profiles. However, for non-uniformly packed columns or process-scale systems with pronounced entrance and exit effects, axial dispersion may indeed become a dominant dispersive force.

Figs. 6–10 simulate various stages in the development of displacement zones in the presence of axial dispersion and finite mass transfer. These patterns are similar to those obtained in ideal displacement chromatography with the concentration shock waves now replaced with dispersed shock layers. The unusual shapes of these zones can be attributed to a combination of chromatographic modes operating simultaneously within the column. Specifically, during the introduction of the feed, multicomponent frontal chromatography is occuring, resulting in the formation of concentration profiles similar to those described by Jacobson *et al.*[32]. Upon the introduction of the displacer at τ_{feed}, the frontal chromatographic patterns are disturbed by the action of the displacer resulting in a development pattern as illustrated in Fig. 6. At this column length, the displacement zone of component 3 begins to form. The displacement of the less adsorbing feed components, 1 and 2, results in the accumulation of these solutes further downstream, leading to the formation of elevated concentration peaks. Fig. 7 depicts the effluent profile for a 20-cm column. At this column length, the displacement zone of component 3 is essentially fully developed while the displacement zones of components 1 and 2 are being formed. Full displacement development is achieved at a column length of 30 cm, as shown in Fig. 8. The effect of mass transfer limitations is clearly seen by the significant amount of zone overlap at full development.

In non-ideal multicomponent adsorption systems, it has been established that constant patterns are obtained with sufficiently long columns[9,35]. These constant patterns result from a dynamic balance of the dispersive and self-sharpening forces acting on the concentration front. Figs. 9 and 10 show the effluent profiles for column lengths of 40 and 50 cm, respectively. It can be seen that the displacement profiles achieved at these two column lengths are identical. Thus, this model predicts that constant pattern formation is also achieved in non-ideal displacement chromatography.

The major goal in process-scale chromatography is to maximize the product throughput, the total mass purified per unit time at a specified purity. Frenz *et al.*[36] have experimentally investigated the optimization of flow-rate, feed load, and

displacer concentration in high-performance displacement chromatography. In our work, we examine the effects of these operating parameters on throughput maximization under conditions of ideal and non-ideal chromatography. Furthermore, we extend the treatment to include the effects of particle diameter and solute diffusivity.

Fig. 11 demonstrates the effect of increasing feed load on the throughput of components 1 and 3 under various conditions of non-ideality. All throughput curves exhibit a maximum at a unique value of the feed volume. At low feed loads, complete development is achieved but the column is "under-utilized" with only a small fraction of the column bed being employed in the separation at a given time. At high feed loads, the column length is insufficient for full development, resulting in incomplete separation of the products and a corresponding decrease in throughput at the elevated mass loadings. The effects of mass transfer are clearly seen in this figure by the reduction of the throughput values with decreasing Stanton numbers. Under non-ideal

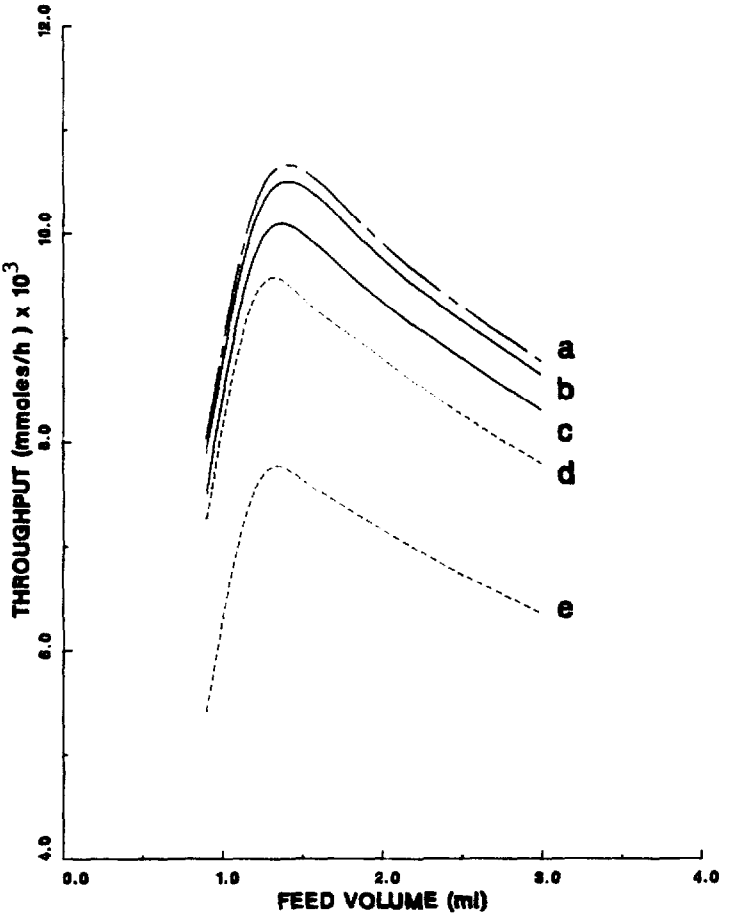

Fig. 11. The effect of feed volume on product throughput. Simulation conditions are described in Table II for runs 11 and 12. a = Components 1 and 3, ideal; b = component 1, St = 800; c = component 1, St = 300; d = component 3, St = 800; e = component 3, St = 300.

displacement conditions, component 1 has a higher throughput than component 3. This is due to the relative position of the components in the displacement train. At full development, component 1 can mix only with component 3, whereas component 3 can mix with both component 1 and the displacer. Furthermore, the equilibrium concentration of component 3 is higher, with a corresponding smaller zone width. This leads to a greater loss of pure material due to zone mixing.

The effect of displacer concentration on product throughput is illustrated in Fig. 12. All data in this figure were generated by using displacer concentrations above 12 mM, the minimum concentration required for displacement of all feed components[7]. The speed of the displacer shock wave is an increasing function of its concentration[5,20]. At low concentrations, the shock wave moves slowly through the column resulting in long separation times and accompanying low throughputs. Ideally, increasing the displacer concentration results in shorter separation times and elevated throughputs. However, this is not the case for non-ideal displacement systems as seen

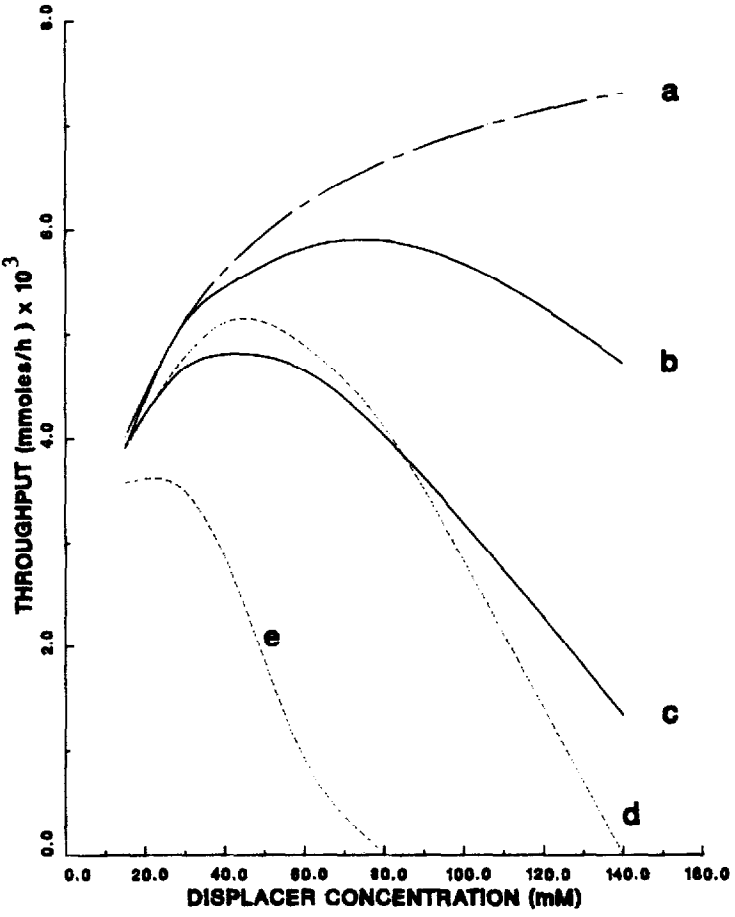

Fig. 12. The effect of displacer concentration on product throughput. Simulation conditions are described in Table II for runs 13 and 14. Symbols as described in Fig. 11.

in Fig. 12. Higher displacer concentrations result in both elevated product concentrations and narrow widths of the displacement zones. Thus, as the displacer concentration increases, mixing due to mass transfer limitations will become increasingly significant. For non-ideal displacement systems, an optimum value of the displacer concentration exists which maximizes the throughput of a given compound.

Fig. 13 illustrates the effect of increasing interstitial velocity on the throughput in both ideal and non-ideal displacement chromatography. In ideal chromatography, the throughput will continue to increase with increasing velocity. In actuality, the throughput decreases at high velocities due to the mass transport limitations and accompanying zone mixing. Thus, an optimal value of the flow-rate exists which maximizes throughput. The theoretical results presented in Figs. 11–13 are in concordance with the experimental results reported by Frenz *et al.*[36].

The influence of mass transfer limitations on product throughput were

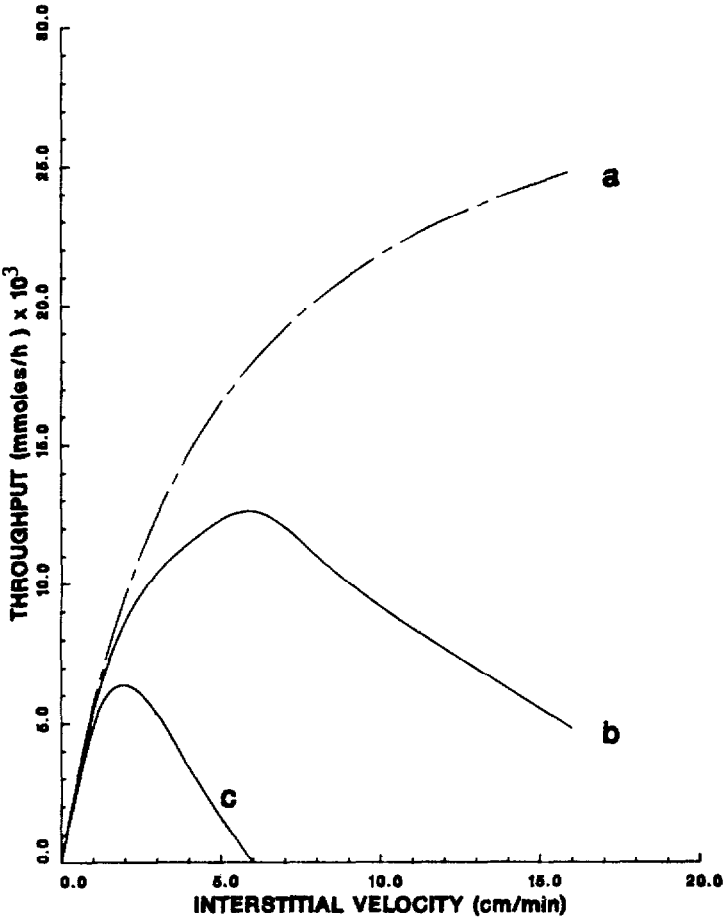

Fig. 13. The effect of interstitial velocity on product throughput. Simulation conditions are described in Table II for run 15. a = Components 1 and 3, ideal; b = component 1, non-ideal; c = component 3, non-ideal.

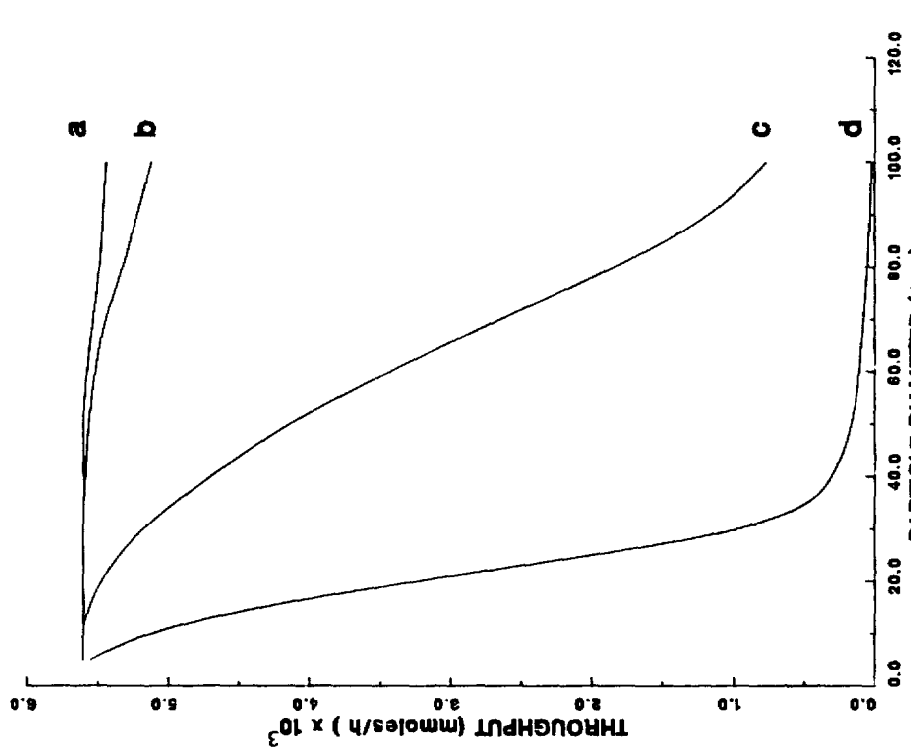

Fig. 14. The effect of particle diameter on product throughput at a constant solute diffusivity of $2 \cdot 10^{-5}$ cm^2/s. Simulation conditions are described in Table II for run 16. u_0: a = 10 cm/min; b = 5 cm/min; c = 1 cm/min.

Fig. 15. The effect of particle diameter on product throughput at a constant interstitial velocity of 1 cm/min. Simulation conditions are described in Table II for run 17. D: a = $4 \cdot 10^{-5}$ cm^2/s; b = $2 \cdot 10^{-5}$ cm^2/s; c = $2 \cdot 10^{-6}$ cm^2/s; d = $2 \cdot 10^{-7}$ cm^2/s.

investigated as a function of particle diameter, interstitial velocity and solute diffusivity. The effects of interstitial velocity and particle diameter on the throughput of component 1 are illustrated in Fig. 14. A constant solute diffusivity of $2 \cdot 10^{-5}$ cm^2/s, typical of small solutes, along with a Stanton number which varied according to eqn. 25 was used to generate this plot. At low velocities, the throughput is essentially independent of particle diameter. The throughput can be dramatically increased by operating at elevated velocities when small particle diameter adsorbents are employed. As the particle diameter increases, however, these advantages become less pronounced. In fact, at large particle diameters, the throughput obtained at high velocities can actually be lower than when operating at lower velocities.

In Fig. 15, the combined effects of solute diffusivity and particle diameter on the throughput are illustrated for a constant interstitial velocity of 1 cm/min. The throughput is insensitive to the particle diameter for small solutes. Thus, large particles can be employed for the separation of relatively small biomolecules with an accompanying reduction in capital costs. On the other hand, as the molecular dimensions of the solute increase, the throughput becomes an increasingly stronger function of the particle diameter. This effect is dramatically shown for a solute diffusivity of $2 \cdot 10^{-7}$ cm^2/s, typical of proteins. Clearly, for the separation of macromolecules by displacement chromatography, it is imperative that small particles be employed.

CONCLUSION

A mathematical model was developed to study the effects of axial dispersion and finite mass transfer in displacement chromatography. While the displacement profile was fairly insensitive to axial dispersion, slow mass transfer rates were shown to have a significant dispersive effect on the concentration shock waves generated in displacement chromatography. In addition, constant pattern formation was obtained under non-ideal conditions. The model was also employed to examine the throughput of these systems as a function of feed load, displacer concentration and interstitial velocity. Under non-ideal conditions, a unique optimum value of these operating parameters existed which maximized the throughput. In order to examine the potential scale-up of the process, the interplay of particle diameter, solute diffusivity, and interstitial velocity was investigated. The results indicated that the use of large particles are potentially detrimental to the performance of displacement systems when high velocities are employed. In fact, macromolecular separations by displacement chromatography may necessitate the use of small particle diameters. The incorporation of adsorption and desorption kinetics along with the experimental evaluation of the model predictions will be the subject of a future report.

SYMBOLS

a_i Langmuir parameter for species i (dimensionless)
b_i langmuir parameter for species i (mM^{-1})
c_{iF} feed concentration for species i (mM)
c_i mobile phase concentration of species i (mM)
D_i effective axial dispersion coefficient of species i (cm^2/s)

D_m solute molecular diffusion coefficient (cm^2/s)
D_p solute intraparticular diffusion coefficient (cm^2/s)
d_p stationary phase particle diameter (cm)
K equilibrium partition coefficient (dimensionless)
k_f film mass transfer coefficient (cm/s)
k_i overall mass transfer coefficient of species i (s^{-1})
L column length (cm)
m axial coordinate of the node within the computational grid (dimensionless)
n temporal coordinate of the node within the computational grid (dimensionless)
N number of components (dimensionless)
Pe_i $u_0 L/D_i$, column Peclet number (dimensionless)
$\bar{q}_i$ average stationary phase concentration of species i (mM)
q_i^* equilibrium stationary phase concentration of species i (mM)
St_i $k_i L/u_0$, Stanton number (dimensionless)
t time (s)
t_{displ} displacer breakthrough time (s)
t_{feed} feed introduction time (s)
u_{min} minimum velocity of any species moving within the column (dimensionless)
u_0 interstitial mobile phase velocity (cm/s)
x z/L, dimensionless axial position
z axial position (cm)
ε fractional void space of fixed bed (dimensionless)
ε_p intraparticular void space (dimensionless)
θ tortuosity factor (dimensionless)
λ parameter which measures flow inequalities in the bed (dimensionless)
τ $u_0 t/L$, dimensionless time
τ_{displ} dimensionless displacer breakthrough time
τ_{feed} dimensionless feed introduction time
ψ dimensionless stability parameter
Ω dimensionless parameter dependent only on interparticulate porosity
ω dimensionless parameter dependent on bed porosity

ACKNOWLEDGEMENT

This work was supported in part by Grant No. CBT-8708799 from the National Science Foundation.

REFERENCES

1 A. Tiselius, *Ark. Kemi, Mineral. Geol.*, 16 (A) (1943) 1.
2 S. M. Cramer and Cs. Horváth, *Prep. Chromatogr.*, 1 (1988) 29.
3 Cs. Horváth, A. Nahum and J. H. Frenz, *J. Chromatogr.*, 218 (1981) 365.
4 Cs. Horváth, J. H. Frenz and Z. El Rassi, *J. Chromatogr.*, 255 (1983) 273.
5 J. H. Frenz and Cs. Horváth, *AIChE J.*, 31 (1985) 400.
6 S. M. Cramer, Z. El Rassi and Cs. Horváth, *J. Chromatogr.*, 394 (1987) 305.
7 Cs. Horváth, in F. Bruner (Editor), *The Science of Chromatography* (*Journal of Chromatography Library*, Vol. 32), Elsevier, Amsterdam, 1985, pp. 179–203.
8 A. W. Liao, Z. El Rassi, D. M. LeMaster and Cs. Horváth, *Chromatographia*, 24 (1987) 881.
9 W. G. Bradley and N. H. Sweed, *AIChE Symp. Ser.*, 71, 152 (1975) 59.

10 A. I. Liapis and D. W. T. Rippin, *Chem. Eng. Sci.*, 32 (1977) 619.
11 M. W. Balzli, A. I. Liapis and D. W. T. Rippin, *Trans. Inst. Chem. Eng.*, 56 (1978) 145.
12 J. S. C. Hsieh, R. M. Turian and C. Tien, *AIChE J.*, 23 (1977) 263.
13 S.-C. Wang and C. Tien, *AIChE J.*, 28 (1982) 565.
14 M. Morbidelli, A. Servida, G. Storti and S. Carra, *Ind. Eng. Chem. Fundam.*, 21 (1982) 123.
15 E. Santacesaria, M. Morbidelli, A. Servida, G. Storti and S. Carra, *Ind. Eng. Chem. Process Des. Dev.*, 21 (1982) 446.
16 F. G. Helfferich and G. Klein, *Multicomponent Chromatography: Theory of Interference*, Marcel Dekker, New York, 1970.
17 F. G. Helfferich, *AIChE Symp. Ser.*, 80, 233 (1984) 1.
18 F. G. Helfferich, *J. Chromatogr.*, 373 (1986) 45.
19 H.-K. Rhee, R. Aris and N. R. Amundson, *Philos. Trans., R. Soc. London Ser. A*, 267 (1970) 419.
20 H.-K. Rhee and N. R. Amundson, *AIChE J.*, 28 (1982) 423.
21 Q. Yu and N.-H. L. Wang, *Sep. Purif. Methods*, 15 (2) (1986) 127.
22 R. W. Geldart, Q. Yu, P. C. Wankat and N.-H. L. Wang, *Sep. Sci. Technol.*, 21 (9) (1986) 873.
23 G. Guiochon and A. Katti, *Chromatographia*, 24 (1987) 165.
24 M. Morbidelli, G. Storti, S. Carra, G. Niederjaufner and A. Pontoglia, *Chem. Eng. Sci.*, 39 (3) (1984) 383.
25 M. Morbidelli, G. Storti, S. Carra, G. Niederjaufner and A. Pontoglia, *Chem. Eng. Sci.*, 40 (7) (1985) 1155.
26 G. Subramanian, M. W. Phillips and S. M. Cramer, *J. Chromatogr.*, 439 (1988) 341.
27 Cs. Horváth and H.-J. Lin, *J. Chromatogr.*, 126 (1976) 401.
28 Cs. Horváth and H.-J. Lin, *J. Chromatogr.*, 149 (1978) 43.
29 J. R. Condor and C. L. Young, *Physicochemical Measurements by Gas Chromatography*, Wiley, New York, 1979.
30 J. Jacobson, J. Frenz and Cs. Horváth, *J. Chromatogr.*, 316 (1984) 53.
31 D. M. Ruthven, *Principles of Adsorption and Adsorption Processes*, Wiley, New York, 1984.
32 J. Jacobson, J. H. Frenz and Cs. Horváth, *Ind. Eng. Chem. Res.*, 26 (1987) 43.
33 H.-K. Rhee and N. R. Amundson, *Chem. Eng. Sci.*, 27 (1972) 199.
34 L. Lapidus and G. F. Pinder, *Numerical Solution of Partial Differential Equations in Science and Engineering*, Wiley, New York, 1982.
35 D. O. Cooney and E. Lightfoot, *Ind. Eng. Chem. Process Des. Dev.*, 5 (1) (1966) 25.
36 J. Frenz, Ph. van der Schrieck and Cs. Horváth, *J. Chromatogr.*, 330 (1985) 1.